Indian J. Phys. **78A** (1), 75-79 (2004)

Nanomaterials–2003

AN INTERNATIONAL JOURNAL IJP A

Formation of gold nanoparticles within surface-functionalized ordered mesoporous molecular sieves

Anirban Ghosh[1]*, Chitta Ranjan Patra[1], Murali Sastry[2] and Rajiv Kumar[1]

[1] Catalysis and [2]Materials Chemistry Divisions, National Chemical Laboratory, Pune-411 008, Maharashtra, India

E-mail : ghosh@ncata.ncl res.in

Abstract : Synthesis and subsequent stabilization of gold nanoparticles within propylthiol-functionalized mesoporous MCM-41 (SH-MCM-41) material is reported. The method, where the chloroaurate ions are reduced *via* surface silanol groups of the SH-MCM-41 material to form uniform-sized gold nanoparticles consequently anchored to the host matrix through the -SH functionality, is quite simple and environmentally benign as there is no need to add any external reducing agent. The nanogold-SH-MCM-41 material is an example of an inorganic-organic hybrid material and was characterized by XRD, UV-Vis, TEM, XPS, XRF, TG-DTA and N_2 adsorption measurements.

Keywords : Gold nanoparticle, ordered mesoporous silica, thiol-functionalized MCM-41.

PACS Nos. : 61.46 +w, 81 07.Pr

1. Introduction

The discovery of ordered M41S type molecular sieves [1,2] has opened up new vistas in catalysis [3] and materials science [4]. The most widely exploited member in the M41S family is MCM-41, which possesses hexagonal packed array of non-interconnecting cylindrical channels. These materials have extremely high surface area (> 1000 $m^2 g^{-1}$) and pore diameter ranging from 2–10 nm, which could be accessible for larger guest molecules [5]. Recently considerable attention has been paid towards surface-modification of these mesoporous materials by reactive organic functional groups such as propylthiol [6], which allows specific control over surface properties [7]. This propylthiol-functionalized MCM-41 (SH-MCM-41) material could be employed as support for metallic [8] and semiconductor nanoparticles [9] to form novel advanced organic-inorganic hybrid materials.

During the past few decades there has been significant interest towards understanding the size-dependent physicochemical properties of gold nanoparticles due to their immense importance in catalysis [10], optoelectronics [11], as novel templates in biomineralization [12], detection of genetic disorders [13], to mention a few. Generally, surfactant molecules containing polar head groups like thiol (-SH), amine ($-NH_2$) *etc.* are used to stabilize nanoparticles to prevent their agglomeration to get the quantum dots [14,15]. The propylthiol-functionalized MCM-41 material possesses the necessary polar head group generally required to stabilize the nanoparticles. Further, they provide a solid support of well-defined pores to the nanoclusters.

However, in most of the reports regarding formation and stabilization of metallic nanoparticles, the hosts used are usually passive and do not participate actively in the reduction of metal ions to form nanoparticles followed by their entrapment in the host matrix [16,17]. Some external method, either chemical (reduction by borohydride, citrate *etc.*) or physical (vapor deposition, lithography *etc.*) has to be employed for the formation of the nanoparticles prior to their stabilization. Realizing the immense importance of nanocomposites in various future applications, we have developed a novel and ecofriendly process for the formation of uniform sized gold nanoparticles and their simultaneous stabilization using propylthiol-functionalized MCM-41 materials in a single step. The -SH groups bind the nanoparticles through covalent interactions, thereby avoiding the requirement of external capping agents for particle size control [14,15].

2. Experimental

2.1. Synthesis of siliceous MCM-41 (Si-MCM-41) :

The Si-MCM-41 material was synthesized with the following initial gel composition, $1.0SiO_2 : 0.32NaOH : 0.21CTABr : 125H_2O$

* Corresponding Author

(CTABr = cetyltrimethylammomium bromide), as described in details elsewhere [18]. The reaction mixture was first stirred at room temperature for 3 h, transferred to a 250 mL polypropylene bottle, and heated at 100°C for 18 h under static condition and autogeneous pressure. After the specified duration, the solid material was recovered by filtration, washed with copious amounts of water and acetone, and calcined at 540°C for 12 h for complete removal of the surfactant.

2.2. Grafting of thiol functionality on Si-MCM-41 surface :

1.0 g of the calcined Si-MCM-41 material was suspended on 30 ml of dry dichloromethane (CH_2Cl_2), 0.03 mL of dichlorodiphenylsilane (Ph_2SiCl_2) was added to this and stirred for 1 h. The contents were then cooled to −78°C and 1.0 mL of 3-mercaptopropyltrimethoxy silane [$(CH_3O)_3Si(CH_2)_3SH$] was added drop wise to this slurry, stirred for further 24 h at 40°C, filtered, washed several times with dry CH_2Cl_2 and dried at ambient temperature under vacuum.

2.3. In situ reduction of chloroaurate ions by SH-MCM-41 material :

1.0 g of the SH-MCM-41 material was treated with 100 mL of 10^{-4} M $HAuCl_4$ solution for 96 h at room temperature. After the specified duration, the solid material was recovered from the mixture, washed thoroughly with copious amounts of water and finally dried under vacuum at room temperature. The material thus obtained after treatment with $AuCl_4^-$ is designated as Au-SH-MCM-41.

2.4. Characterization of the materials :

Low angle powder X-ray diffraction (XRD) patterns of the calcined Si-MCM-41 and SH-MCM-41 materials were recorded on a Rigaku D Max III VC instrument with Ni filtered Cu K_α radiation (λ = 1.5404 Å) in the 2θ range of 1.5–10° at a scan rate of 1°/min. The specific surface areas of the SH-MCM-41 and Au-SH-MCM-41 samples were determined by the BET method [19] from N_2 adsorption isotherms at −196°C using an Omnisorb CX-100 Coulter instrument. Prior to the adsorption experiment, the samples were activated at 150°C for 6 h at 1.333×10^{-2} Pa. Pore size distribution of the samples was computed by Barrett-Joyner-Halenda (BJH) model [20]. Chemical analysis of the SH-MCM-41 material was done on a Carlo Erba EA1108 elemental analyzer.

The UV-Vis spectra of the parent SH-MCM-41 and Au-SH-MCM-41 hybrid materials were recorded on a Shimadzu UV-2101PC spectrophotometer operating on reflection mode at a resolution of 2 nm using barium sulphate as a standard for background correction. To determine the size of the gold nanoparticles, XRD patterns of the Au-SH-MCM-41 hybrid material were recorded on a Philips PW 1830 instrument operating at 40 kV voltage and a current of 30 mA with Cu K_α radiation between 2θ ranges 30° and 45° at a scan rate of 1°/min; and the mean diameter was calculated by applying Debye-Scherrer equation [21]. The Au-SH-MCM-41 sample was dispersed by acetone on Holey carbon grids and transmission electron microscopic (TEM) images were scanned on a Jeol Model 1200 EX instrument operated at an accelerating voltage of 100 kV. The X-ray photoelectron spectra (XPS) of the Au-SH-MCM-41 hybrid material was recorded on a VG MicroTech ESCA 3000 instrument at a pressure better than 1.333×10^{-7} Pa. The general scan and C 1*s*, S 2*p*, Si 2*p* and Au 4*f* core level spectra were recorded with unmonochromatized Mg K_α radiation (photon energy = 1253.6 eV) at pass energy of 50 eV and electron takeoff angle (angle between electron emission direction and surface plane) of 60°. The overall resolution of XPS measurement was thus ~ 1 eV. The core level spectra were background corrected using the Shirley algorithm [22] and the chemically distinct species resolved using a non-linear least squares procedure. The core level binding energies were aligned with respect to the Au $4f_{7/2}$ binding energy of 84 eV. X-Ray fluorescence (XRF) measurement of the Au-SH-MCM-41 material was performed on a Rigaku 3070 sequential wavelength dispersive spectrophotometer, with a rhodium target energized at 50 kV and 40 mA. The thermogravimetric and differential thermal analyses (TG-DTA) of the SH-MCM-41 and Au-SH-MCM-41 materials were performed on a Seiko Instruments model TG/DTA 32 at a heating rate of 10°C/min.

3. Results and discussion

3.1. N_2 adsorption and desorption :

The specific BET surface area, pore volume and mean pore diameter calculated from the N_2 adsorption isotherms using the BJH model for all the mesoporous samples are summarized in Table 1. All the samples showed isotherms of type IV in the IUPAC classification [23] having a sharp capillary condensation step at around P/P_0 = 0.3–0.45 region without hysteresis between

Table 1. The BET surface area (SA), mean pore diameter (PD), pore volume (PV), d_{100}, a_0, framework thickness (FWT), and results of elemental analyses for SH-MCM-41 and Au-SH-MCM-41

Sample[a]	SA ($m^2\ g^{-1}$)	PD (Å)	PV ($cm^3\ g^{-1}$)	d_{100} (Å)	a_0 (Å)[b]	FWT (Å)[c]	S (mmol g^{-1})	Au (mmol g^{-1})[d]
A 883	36.79	1.01	40.11	46.31	9.52	3.21	–	
B 689	36.65	0.79	39.94	46.12	9.47	3.20	0.62	

[a]A = SH-MCM-41, B = Au-SH-MCM-41. [b]$a_0 = 2d_{100}/\sqrt{3}$. [c]FWT = a_0 − PD. [d]From XRF.

he adsorption and desorption branches, characteristic of M41S ype ordered mesoporous materials [24]. The nature of the N_2 dsorption isotherms remained the same even after *in situ* eduction of $AuCl_4^-$ ions by the mesoporous sample, but ecreases of 22 % in the surface area and in the pore volume of u-SH-MCM-41 were observed. However, the average pore ameters of the sample after entrapment of Au nanoparticles id not change considerably. All the results indicate partial filling f the mesoporous channels by gold nanoparticles without much lteration in the mesoporosity.

.2. *Optical properties :*

igure 1 shows the UV-Vis spectra recorded from the (a) parent H-MCM-41 and (b) Au-SH-MCM-41. A strong absorption at a. 540 nm is observed for all the mesoporous materials after eatment with $HAuCl_4$ solution and is a clear indication of eduction of the $AuCl_4^-$ ions. Au nanoparticles have a haracteristic absorption band in the visible region of the lectromagnetic spectrum at around 520–550 nm due to surface lasmon vibrations, which is responsible for the striking violet pink range of colors depending upon particle size [25,26]. his resonance is absent in the parent SH-MCM-41 material as xpected. An additional resonance at *ca.* 725 nm was observed case of the Au-SH-MCM-41 (Figure 1, curve b) material, arose om excitation of longitudinal surface plasmon vibrations due close packing of the gold nanoparticles [27,28] within the esoporous channels, resulted from anchoring of the gold anoparticles to the surface of siliceous matrices by the thiol roups.

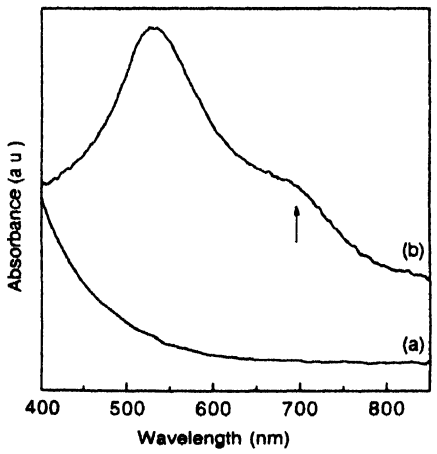

ure 1. UV-Vis spectra recorded from the (a) SH-MCM-41 and (b) Au-I-MCM-41 materials.

3. *X-ray diffraction :*

gure 2 shows the low angle powder X-ray diffraction patterns (a) Si-MCM-41, (b) SH-MCM-41 and (c) Au-SH-MCM-41, in hich the main (100) Bragg reflection along with the weak (110), 0) and (210) reflections are well visible, indicating high degree ordered hexagonal mesopores even after *in situ* formation of ld nanoparticles within the cavities. The d_{100} values along with the corresponding unit cell parameter (a_0) of the different MCM-41 samples are given in Table 1. The a_0 values are calculated by the equation $a_0 = 2d_{100}/\sqrt{3}$.

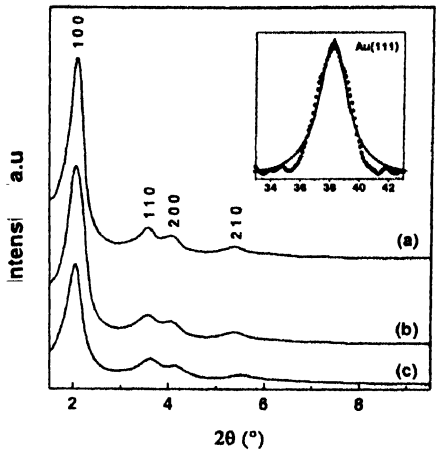

Figure 2. Powder X-ray diffraction patterns of (a) Si-MCM-41, (b) SH-MCM-41 and (c) Au-SH-MCM-41 materials. Inset shows diffraction pattern of Au-SH-MCM-41 material in the region of the Au(111) Bragg reflection at 2θ = 38.2°, the solid line being the Lorentzian fit to the curve.

The diffraction patterns of the Au-SH-MCM-41 material in the 2θ range of 30–45° are shown in inset of Figure 2, the solid line being the Lorentzian fit to the curve. Under the experimental conditions of the XRD experiments (small slit width and monochromatized Cu K_α radiation), it was felt that the XRD line-shape would be better approximated by a Lorentzian than a Gaussian. Indeed, poorer chi-square error values (which denote the goodness of fit) were observed while fitting the Au(111) Bragg reflection to a Gaussian. The mean diameter of the gold nanoparticles was calculated by applying Debye-Scherrer equation from the broadening of the Au(111) Bragg reflection at 2θ = 38.2°, which yielded the value of *ca.* 3.2 ± 0.5 nm. This value is in accordance with the maximum possible particle size that can fairly be accommodated within the channels of SH-MCM-41 having mean pore diameter ~3.7 nm (Table 1).

3.4. Transmission electron microscopy :

The TEM image of the Au-SH-MCM-41 sample is given in Figure 3, inset showing selected area electron diffraction pattern.

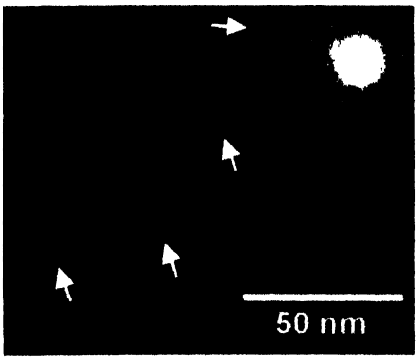

Figure 3. Transmission electron micrograph of the Au-SH-MCM-41 material. The gold nanoparticles are highlighted by arrows in the figure. Inset shows selected area electron diffraction pattern.

The parallel fringes due to side-on view of the long pores of MCM-41 are well visible in the image. The selected area electron diffraction pattern of the sample exhibits well-defined hexagonal maxima, further confirming periodicity of the structure. The entrapped gold nanoparticles are highlighted by arrows in the figure. The spatial distribution of the nanoparticles to the perpendicular direction of the channels was observed to be consistent with pore spacing.

3.5. Chemical characterization of the samples :

Results of elemental analyses and XRF measurements are summarized in Table 1. Figure 4 shows the X-ray photoelectron spectra recorded from the Au-SH-MCM-41 material, insets being the S 2*p* and Au 4*f* core level spectra. Strong signals from the gold nanoparticles entrapped in the mesoporous network were observed. These core levels could be fit to a single spin-orbit pair indicating no chemical shifts arising due to complexation with -SH groups in the MCM-41 matrix. The S 2*p* signal from the Au-SH-MCM-41 sample could be satisfactorily fit to a single spin-orbit pair separated by 1.14 eV. It is interesting to note the absence of an additional high binding energy component in the S 2*p* spectrum at *ca.* 168 eV that is often observed in self-assembled monolayers of alkanethiols on silver alloy surfaces [29], which indicates that the thiol groups are not oxidized to a sulfonate species and complexation with gold nanoparticles stabilizes them.

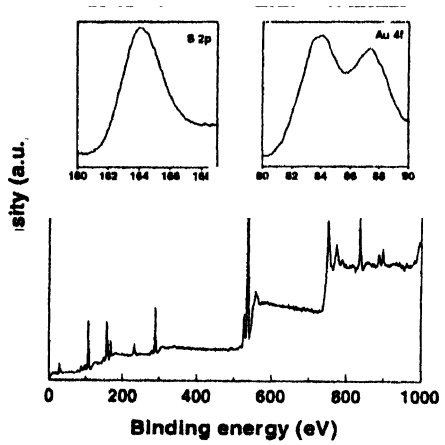

Figure 4. X-ray photoelectron spectra recorded from the Au-SH-MCM-41 material. Insets show the S 2*p* and Au 4*f* core level spectra.

3.6. Thermal analyses :

Figure 5 (left axes) shows the TGA data recorded for the (A) parent SH-MCM-41, and (B) Au-SH-MCM-41 materials. The major features in the TGA curves for the two materials are almost similar. The significant weight loss at *ca.* 330°C in both the cases can be attributed to decomposition of the -SH groups from the framework. Significant differences are observed in the DTA curves (Figure 5, right axes) for the (A) parent and (B) Au-SH-MCM-41 materials in the high temperature region. An exothermic process is observed at *ca.* 440°C for the Au-SH-MCM-41 material (Figure 5B, right axis) which is clearly absent in the parent material (Figure 5A, right axis). This exothermic process is not accompanied by a detectable weight loss as observed in the TGA data. This exothermic reaction occurred due to sintering of the gold nanoparticles within the porous framework. The decomposition of the thiol groups at *ca.* 330°C facilitates diffusion of the free Au nanoparticles within the porous network and thereafter, sintering. This clearly indicates cross-linking of the colloidal gold nanoparticles, which opens a new strategy for the formation of superstructures of nanoparticles with controllable geometry.

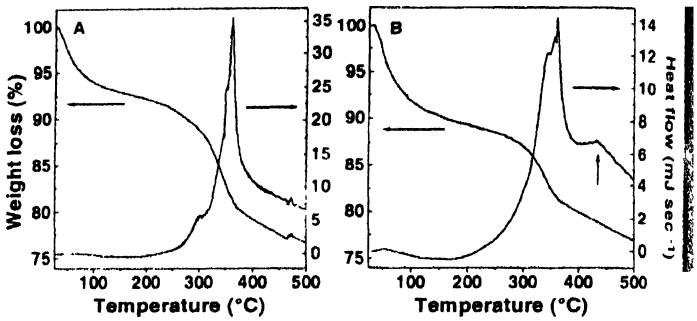

Figure 5. TGA (left axes) and DTA data (right axes) recorded for (A) the SH-MCM-41 and (B) the Au-SH-MCM-41 materials.

3.7 Probable pathway for the formation of gold nanoparticles

It is pertinent here to mention the work of Esumi *et al* [30], who have demonstrated that the spontaneous reduction of chloroaurate ions by sugar balls (sugar persubstituted poly(amidoamine) dendrimers) occurs *via* the hydroxyl groups present on the outer surface; the hydroxyl groups being converted to carbonyl groups thereafter. However the silanol groups of the surfaces of MCM-41 cannot be oxidized further, and exact mechanism of the nanoparticle formation requires further work to be understood. But the participation of the silanol groups in the reduction process can be established from the fact that amorphous (fumed) silica can also form surface bound gold nanoparticles in similar conditions, and concentration of gold on silica depends on the number of silanol groups present on the silica surface [31].

4. Conclusion

From the results it can be concluded gold nanoparticles can be conveniently synthesized and stabilized in ordered mesoporous siliceous matrices. The silanol groups present on the surface of host matrices participate in the reduction of aqueous chloroaurate ions to form the nanoparticles. The pendant -SH functional groups residing deep inside the mesopores serve subsequently entraps the gold nanoparticles through covalent interactions just after their formation, thereby perfectly accommodating them inside the pores. The mean diameter of the supported nanoparticles falls in the particular size range (2-5 nm) where gold nanoparticles show excellent catalytic activity in variety of reactions. Hence our approach for the preparation of supported gold nanoparticles on siliceous matrices offers

distinct advantages in exploiting the catalytic potential of these materials.

Acknowledgments

AG and CRP gratefully acknowledge Council of Scientific and Industrial Research, New Delhi, Government of India, for grant of research fellowships. We thank Dr. P Mukherjee for helpful discussions.

References

[1] C T Kresge, M E Leonowicz, W J Roth, J C Vartuli and J S Beck *Nature* **359** 710 (1992)

[2] J S Beck, J C Vartuli, W J Roth, M E Leonowicz, C T Kresge, K D. Schmitt, C T -W Chu, D H Olson, E W Sheppard, S B McCullen, J B Higgins and J L Schlenker J *Am. Chem Soc.* **114** 10834 (1992)

[3] A Corma *Chem. Rev.* **97** 2373 (1997)

[4] Y Sakamoto, M Kaneda, O Terasaki, D Zhao, J M Kim, G D Stucky, H J Shin and R Ryoo *Nature* **408** 449 (2000)

[5] K Moller and T Bein *Chem. Mater.* **10** 2950 (1998)

[6] X Feng, G E Fryxell, L -Q Wang, A Y Kim, J Liu and K M Kemner *Science* **276** 923 (1997)

[7] A Stein, B J Melde and R C Schroden *Adv Mater.* **12** 1403 (2000)

[8] P Mukherjee, M Sastry and R Kumar *Phys. Chem. Comm.* **3** 15 (2000)

[9] T Hirai, H Okubo and I Komasawa *J. Phys. Chem.* **B103** 4228 (1999)

[10] M Valden, X Lai and D W Goodman *Science* **281** 1647 (1998)

[11] G Markovich, C P Collier, S E Henrichs, F Remacle, R D Levine and J R Heath *Acc Chem. Res.* **32** 415 (1999)

[12] J Kunther, R Seshadri, G Nelles, W Assenmacher, H -J. Butt, W Mader and W Tremel *Chem. Mater.* **11** 1317 (1999)

[13] S -J Park, T A Taton and C A Mirkin *Science* **295** 1503 (2002)

[14] M Brust, M Walker, D Bethell, D J Schiffrin and R Whyman *J. Chem Soc., Chem. Commun.* 801 (1994)

[15] D V Leff, L Brandt and J R Heath *Langmuir* **12** 4723 (1996)

[16] Y Sun and Y Xia *Science* **298** 2176 (2002)

[17] A Kumar, P Mukherjee, A Guha, S D Adyantaya, A B Mandale, R Kumar and M Sastry *Langmuir* **16** 9775 (2000)

[18] K Mukhopadhyay, A Ghosh and R Kumar *Chem. Commun.* 2404 (2002)

[19] S Brunauer, P H Emmett and E Teller *J. Am. Chem. Soc.* **60** 309 (1938)

[20] E P Barrett, L G Joyner and P P Halenda *J. Am. Chem. Soc.* **73** 373 (1951)

[21] R C Rau *Advances in X-ray analysis*, ed W. M. Mueller (London : Sir Isaac Pitman & Sons Ltd.) **Vol 5**, p104 (1962)

[22] D A Shirley *Phys. Rev.* **B5** 4709 (1972)

[23] S J Gregg and K S W Sing *Adsorption, Surface Area and Porosity* (London : Academic Press) Ch 3 p121 (1967)

[24] C -Y Chen, H -X Li and M E Davis *Microporous Mater* **2** 17 (1993)

[25] S Underwood and P Mulvaney *Langmuir* **10** 3427 (1994)

[26] S Link and M A El-Sayed *J. Phys. Chem.* **B103** 4212 (1999)

[27] C G Blatchford, J R Campbell and J A Creighton *Surf. Sci* **120** 435 (1982)

[28] K S Mayya, V Patil and M Sastry *Langmuir* **13** 3944 (1997)

[29] K Bandyopadhyay, K S Mayya, K Vijayamohanan and M Sastry *J. Electron Spectrosc. Relat Phenom.* **87** 101 (1997)

[30] K Esumi, T Hosoya, A Suzuki and K Torigoe *Langmuir* **16** 2978 (2000)

[31] P Mukherjee, C R Patra, A Ghosh, R Kumar and M Sastry *Chem. Mater* **14** 1678 (2002)